Phytomedicine 154 (2026) 158016

Contents lists available at ScienceDirect

Phytomedicine

journal homepage: www.elsevier.com/locate/phymed

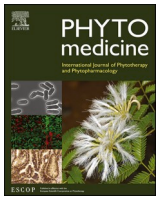

Original Article

Naturally derived Erythrinin C targets γ-secretase signaling to suppress triple-negative breast cancer progression and reverse paclitaxel resistance

Ke-Fan Yang [a,1], Di Wang [b,1], Kuo Yao [a], Ran Xu [a], Li-Zhi Hu [a], Yue-Yang Liu [c], Lu Zhang [c], Qian Xu [c], Xin Yang [d,*], Ming-Sheng Zhou [c,*], Hui Jia [e,*]

[a] Department of Pathology and Pathophysiology, School of Basic Medical Sciences, Shenyang Medical College, Shenyang 110034, China
[b] Department of Pathology, General Hospital of Northern Theater Command, Shenyang 110015, China
[c] Science and Experimental Research Center of Shenyang Medical College, No 146 Huanghe North Street, Yuhong District, Shenyang City 110034, Liaoning Province, China
[d] Department of Endocrinology, General Hospital of Northern Theater Command, Shenyang 110015, China
[e] School of Traditional Chinese Medicine, Shenyang Medical College, No 146 Huanghe North Street, Yuhong District, Shenyang City 110034, Liaoning Province, China

ARTICLE INFO

Keywords:
Erythrinin C
γ-secretase inhibitor
Triple-negative breast cancer
Paclitaxel resistance

ABSTRACT

Background: Triple-negative breast cancer (TNBC) is a highly aggressive subtype of breast cancer. Paclitaxel (Taxol) serves as a first-line chemotherapeutic agent, but the emergence of drug resistance often limits its clinical efficacy. Bioactive compounds with anticancer potential and reduced toxicity have thus gained increasing research interest. Erythrinin C (EC), known for its favorable drug-like properties and accessible sourcing has attracted significant attention. However, its mechanism of action and role in modulating chemotherapy resistance remain unclear.

Purpose: This study aimed to evaluate the antitumor effects of EC on TNBC both *in vivo* and *in vitro*, and to investigate its ability to reverse of drug resistance in TNBC/Taxol cells either alone or in combination with Taxol.

Methods: The crystal structure of the γ-secretase protein was obtained from the Protein Data Bank (RCSB PDB), and a pharmacophore model was constructed based on its natural small-molecule ligands. Pharmacophore-based screening was performed across traditional Chinese medicine and natural product database to identify potential drug candidates. Confirm the interaction target between EC and γ-secretase was validated, and the biological effects, genetic influences, and *in vivo* activity of EC targeting γ-secretase were assessed through *in vitro* and *in vivo* experiments.

Results: EC was identified as a γ-secretase inhibitor and was shown to suppress TNBC cell proliferation and migration *in vitro*. Genetic modulation of PSEN-1 in MDA-MB-231 cells revealed that low PSEN-1 expression inhibits the malignant phenotype of TNBC cells. Pharmacological evaluation confirmed that EC treatment effectively slows TNBC progression. Furthermore, EC effectively reversed Taxol resistance in TNBC/Taxol cells. *In vivo* experiments further demonstrated that the combination of EC and Taxol significantly inhibited xenograft tumor growth.

Conclusion: EC acts as a natural γ-secretase inhibitor that exerts significant anti-TNBC activity in both *in vitro* and *in vivo* by targeting PSEN-1 subunit. It also reverses TNBC/Taxol resistance at both cellular and animal levels, highlighting its promising and potential as a novel targeted therapeutic candidate for TNBC.

Abbreviations: EC, Erythrinin C; HTVS, high-throughput virtual screening; KD, knockdown; LDH, lactate dehydrogenase; NICD, Notch intracellular domain; OE, overexpression; PSEN-1, presenilin; SP, standard precision; TNBC, Triple-negative breast cancer; Taxol, Paclitaxel; XP, extra precision.

* Corresponding authors.
E-mail addresses: zhanglu0412@symc.edu.cn (L. Zhang), xuqiandoctor@sina.com (Q. Xu), kandy15@126.com (X. Yang), zhoums1963@163.com (M.-S. Zhou), huijia412413@symc.edu.cn (H. Jia).
[1] Co-first Author

https://doi.org/10.1016/j.phymed.2026.158016
Received 26 October 2025; Received in revised form 19 February 2026; Accepted 23 February 2026
Available online 26 February 2026

Introduction

Triple-negative breast cancer (TNBC) is the most aggressive subtype of breast cancer and is associated with a poor prognosis (Wang et al., 2024a). Taxol, as a first-line chemotherapy drug for TNBC, demonstrates significant initial efficacy, but its long-term therapeutic effect is hampered by the development of drug resistance, leading to treatment failure and recurrence (Wang et al., 2022). Consequently, enhancing the efficacy of Taxol and overcoming drug resistance are critical clinical goals (Feng et al., 2024). Currently, chemotherapy remains the core of standard clinical treatment for TNBC (Zhang et al., 2025). First-line regimens typically employ taxanes such as paclitaxel (Jiang et al., 2024), docetaxel (Sharma et al., 2024), combined with anthracyclines (epirubicin), which can induce initial responses in some patients (Bianchini et al., 2022). For patients with BRCA1/2 mutations, PARP inhibitors (*e.g.*, olaparib) offer a targeted treatment option (Tutt et al., 2021). Additionally, for PD-L1-positive advanced TNBC, immune checkpoint inhibitors (*e.g.*, atezolizumab) combined with chemotherapy have been incorporated into first-line therapy (Kwapisz, 2021). However, the application of these therapies faces significant limitations. Chemotherapy drugs commonly cause severe side effects, such as bone marrow suppression, neurotoxicity, and cardiotoxicity, which severely impact patients' quality of life (Zheng et al., 2025). More critically, TNBC patients are highly prone to developing acquired drug resistance, leading to treatment failure and disease recurrence.

Screening for bioactive compounds with novel mechanisms of action from natural products, particularly plant-derived medicines, demonstrates unique advantages. Plant-derived compounds typically exhibit structural diversity, multi-target effects, and relatively low toxicity, laying the foundation for discovering novel anticancer lead compounds (Roichman et al., 2025). Multiple studies have confirmed the therapeutic potential of specific plant components in TNBC. Curcumin induces apoptosis in TNBC cells and reverses epithelial-mesenchymal transition by inhibiting NF-κB and Wnt/β-catenin signaling pathways (Tanaka et al., 2018). Resveratrol modulates SIRT1 and AMPK pathways to suppress cell proliferation and enhance chemotherapy sensitivity (Zhang et al., 2025). Green tea polyphenol EGCG exerts anti-TNBC effects by regulating miRNA expression and inhibiting angiogenesis (Fernandes et al., 2018). These studies validate the feasibility of herbal medicines as therapeutic strategies for TNBC and reveal the importance of regulating key signaling pathways in overcoming drug resistance. Notably, the γ-secretase/Notch signaling pathway plays a central role in the development and treatment resistance of TNBC by maintaining tumor stem cell characteristics, promoting epithelial-mesenchymal transition, and mediating chemotherapy resistance (Jia et al., 2021). However, current inhibitors targeting this pathway (γ-secretase inhibitors) often exhibit severe side effects (such as gastrointestinal toxicity) or limited efficacy. Furthermore, plant-derived γ-secretase inhibitors remain understudied in the context of TNBC. Recent studies have revealed that active components in traditional Chinese medicine, known for their high efficacy and low toxicity, represent a promising source for developing novel anticancer drugs (Liang et al., 2023). Therefore, this underscores the urgent need to identify and develop naturally sourced small-molecule targeted drug candidates capable of reversing TNBC resistance.

The Notch pathway is a key driver of chemotherapy resistance in TNBC (Zhu et al., 2023). Notch pathway activation requires the sequential cleavage of notch receptors by Furin-like proteases, a disinterring and metalloproteinase proteases and γ-secretase. The cleavage of the Notch receptor results in the release of the Notch intracellular domain (NICD), which translocate to nucleus, binds transcription factor CSL and recruits co-factors to initiate gene transcription, thereby triggering downstream biological responses (Yao et al., 2024). γ-secretase serves as the terminal cleaving enzyme within the transmembrane region of the Notch pathway and is essential for Notch signal activation. It is a transmembrane protein complex located in the cell membrane, composed of four key subunits: presenilin (PSEN-1/-2), nicastrin, anterior pharynx defective-1, and presenilin enhancer-2 (Yang et al., 2024). Among these, PSEN-1 carries the primary catalytic function, and its activity reflects the hydrolytic function of γ-secretase.

EC is an isoflavone isolated from *Erythrina suberosa* var. In TNBC cells, EC has been shown to inhibit TNBC proliferation and reduce cell viability; however, the underlying mechanism remains unclear. We discovered that EC inhibits γ-secretase activity, with its active moiety exhibiting strong affinity for γ-secretase. In this study, we constructed a pharmacophore model based on the crystal structure of the γ-secretase and its small-molecule natural ligands. Using this model, we systematically screened databases of active components from traditional Chinese medicine and natural products to identify novel drug candidates with potential therapeutic interventions. Building upon this, we employed TNBC cells with either PSEN-1 overexpression (OE) or knockout (KD) through genetic manipulation, along with xenograft tumor models, to evaluate EC's ability to slow TNBC progression by regulating g-secretase. Through cellular phenotype experiments, we demonstrated that EC effectively reversed Taxol resistance in TNBC/Taxol cells.

Materials and methods

Reagents and instruments

The compound Erythrinin C (HY-N3857, CAS No. 63807-85-2, purity: 98.0 %) was sourced from MedChemExpress (Shanghai, China) (Tanaka et al., 2018). Paclitaxel (Taxol, Cat. No MB1178) was obtained from Meilunbio (Dalian, China). Taxol was used as the positive control drug. The following antibodies were used in this study: anti-PSEN-1 (Rabbit mAb #DF6910) from Affinity (Jiangsu, China); anti-Notch1 (Rabbit mAb #3608) from Cell Signaling Technology (Massachusetts, USA); anti-Notch3 (Rabbit mAb #711007) and anti-Notch4 (Rabbit mAb #PA5-96995) from Thermo Fisher Scientific (Massachusetts, USA); anti-BCRP (ABCG2, Rabbit mAb #42078), anti-MDR1 (ABCB1, Rabbit mAb #13342), and anti-CYP3A4 (Rabbit mAb #13384) from Cell Signaling Technology (Massachusetts, USA).

Primary experimental instruments include: CO_2 incubator, Qingdao Haier Co., Ltd.; Fluorescence microplate reader, BMG GmbH, Germany; Chemiluminescent gel imaging system, Aplegen, USA; Inverted microscope, Leica Microsystems GmbH, Germany; Upright fluorescence microscope, Leica Microsystems GmbH, Germany; Microtome, Leica Microsystems GmbH, Germany; Constant-temperature Dry Bath, Beijing Dalong Xingchuang Laboratory Instrument Co., Ltd.; Bench-top Low-speed Centrifuge, Hunan Hesi Instrument Equipment Co., Ltd.; Freeze Centrifuge, Thermo Fisher Scientific, USA; Laminar Flow Hood, Shanghai Longyue Instrument Equipment Co., Ltd.; Slide Mounting and Drying Machine, Hubei Huida Instrument Co., Ltd.; Portable Small Animal Anesthesia Machine, Shenzhen Ruowei Life Technology Co., Ltd.; Ice maker, Panasonic Cold Chain (Dalian) Co., Ltd.; Ultrasonic cell disruptor, Ningbo Xinzhi Biotechnology Co., Ltd.; Autoclave, Xiamen Zhiwei Instruments Co., Ltd.; Agilent NovoCyte flow cytometer, Agilent Technologies, USA; Vertical electrophoresis chamber for protein electrophoresis, BIO-RAD Laboratories, Inc., USA.

Cell culture

The human triple-negative breast cancer cell line MDA-MB-231 was cultured in DMEM medium supplemented with 10 % fetal bovine serum and 1 % penicillin-streptomycin. Its paclitaxel-resistant variant, MDA-MB-231/Taxol was cultured in RPMI 1640 medium supplemented with 10 % fetal bovine serum and 1 % penicillin-streptomycin. All cells were maintained in a humidified incubator at 37 °C with 5 %.

Pharmacophore-based screening for γ-secretase inhibitors

The crystal structure of the PSEN-1 (PDB ID: 6LR4, Chain B) was

obtained from the RCSB PDB database. We prepared protein structure using the Protein Wizard module in Schrödinger Suite, which involved restoring the native ligand conformation, optimizing of hydrogen bonding network, and performing energy minimization, all water molecules were removed from the structural. The ADME/T properties of the compound were predicted using QikProp module. Subsequently, the preprocessed ligand library was subjected to a hierarchical molecular docking workflow against the PSEN-1 active site. This process employed high-throughput virtual screening (HTVS), followed by standard precision (SP), and extra precision (XP) docking modes to progressively refine the screening accuracy. Finally, the binding free energy of top-ranked ligand-PSEN-1 complex was calculated using MM-GBSA method (Wang et al., 2024b).

Molecular docking of EC with PSEN-1

The compound EC was sketched in 2D using Chem-Bio-Draw Ultra 13.0 and converted to a 3D structure using ChemBio3D Ultra 13.0. Ligand preparation was performed using the Lig-Prep module within the Schrödinger Suite, applying the same force field used for receptor optimization. Molecular docking was performed using the Glide module in Schrödinger Maestro 2018 to bind EC into the active site of γ-secretase (PDB code: 6LR4). The built-in 'Protein-Ligand Interaction Diagram' feature was employed for preliminary identification of interactions such as hydrogen bonds and hydrophobic contacts. To generate a high-quality three-dimensional docking diagram, the complex structure was imported into PyMOL 2.5.0 (The PyMOL Molecular Graphics System) for rendering, illustrating the spatial position of the ligand within the binding pocket. To clearly display key interatomic interactions, a two-dimensional interaction diagram was generated using LigPlot+ *v*.2.2 software. This software automatically identifies interactions based on the following criteria: hydrogen bonds (donor-acceptor atom distance $\leq$3.5 Å and donor-hydrogen-acceptor angle $\geq$120°); hydrophobic interactions (nonpolar atom-nonpolar atom distance $\leq$4.0 Å, primarily involving carbon atoms). The two-dimensional chemical structures of ligands were drawn using ChemDraw Professional 20.0 (Bisht et al., 2024). All software was used with default parameters for analysis and plotting.

Western blotting

Cells were harvested, washed once with PBS buffer, and lysed using a RIPA buffer supplemented with protease and phosphatase inhibitors. The lysates were centrifuged at 12,000 g for 15 min to collect supernatant. Total protein concentration was determined using a BCA assay, and 60 μg of protein was loaded per lane for western blot analysis. The target protein and its internal control protein were processed simultaneously in adjacent lanes on the same gel. Equal amounts of protein were separated by electrophoresis on a 10 % SDS-PAGE and subsequently transferred onto a PVDF membrane. The membrane was then blocked with 5 % skim milk TBS for 2 h at room temperature to prevent non-specific binding. Following blocking, the membranes were incubated overnight at 4 °C with the following primary antibodies. After washing with TBST, the membrane was incubated with corresponding horseradish peroxidase labeled secondary antibody for 1 h at room temperature. Protein bands were visualized using an enhanced chemiluminescence substrate and detected using a chemiluminescence imaging system(1800047S). β-actin was used as a loading control protein (Liu et al., 2022). Quantitative analysis of Western blot bands was performed independently by two researchers who were unaware of the experimental groupings.

RT-qPCR analysis

Total RNA was extracted from treated cells using Trizol reagent (1 mL/vial) and purified, an RNA extraction kit (Transgene) according to the manufacturer's instructions. and measure the RNA concentration and purity were measured using a spectrophotometer. Subsequently, 1mg of total RNA was reversed-transcribed into cDNA using the All-in-One First-Strand cDNA Synthesis Kit (Transgene). Quantitative real-time PCR was performed using a standard SYBR Green protocol. The primer sequences used for the target gene PSEN-1 are as follows: forward: AGCACAGAAAGGGAGTCACAAGA; reverse: GTGTAGAGCGATGAGGCCCTAG. PCR amplification conditions consisted of an initial denaturation at 95 °C for 30 s, followed 40 cycles of denaturation at 95 °C for 5 s, and annealing/extension at 60 °C for 30 s. A melting curve analysis was performed at the end of each run to conform amplification specificity. The comparative Ct ($2^{-\Delta\Delta CT}$) method was used to calculate relative mRNA expression, with GAPDH serving as the internal reference gene (Zucha et al., 2021).

Immunofluorescence staining

Cells were treated with EC (5, 10, and 15 μM), Taxol (100 nM), or a combination of EC (10 μM) and Taxol for 48 h. After treatment, cells were washed three washes with PBS and fixed with 4 % paraformaldehyde for 15 min at room temperature. The cells were the permeabilized with 0.2 % Triton X-100 for 5 min and blocked with 5 % BSA for 30 min. Following the blocking, cells were incubated with the following primary antibodies diluted in 1 % BSA overnight at 4 °C: After washed three times with PBS, cells were incubated with the secondary antibody for 1 h at room temperature. Nuclei were counterstained with DAPI for 7 min, and washed three times with PBS. An anti-fluorescence quencher was applied. Images were acquired using a fluorescence microscope (Harms et al., 2023).

Cell viability assay

Cell viability was assessed using the MTT assay. Following a 48 h treatment with various concentrations of EC (1.5625, 3.125, 6.25, 12.5, 25, and 50 μM) for 48 h, MTT solution was added to the cells and then incubated for additional 4 h. Subsequently, 100 μl of dimethyl sulfoxide was added to each well. The plate was incubated for 10 min in an enzyme-linked immunosorbent assay reader, and the optical density was measured at 450 nm (Wang et al., 2023). The results were plotted as a curve, and the IC_{50} value of EC was calculated using GraphPad Prism 9.0 software.

Colony formation assay

After a 48 h incubation in a medium containing EC (5, 10, and 15 μM), Taxol (100 nM), or EC (10 μM) combined with Taxol, the treatment medium was replaced with a complete medium and, the cells were cultured for another 10 days to allow colony formation. The resulting colonies were then washed once with PBS, fixed with 4 % formaldehyde solution for 15 min, and stained with 0.1 % crystal violet for 8 min. Finally, the plates were washed three times with PBS, air-dried at room temperature, and photographed (Yang et al., 2023).

Tumor spheroid formation

Cells were incubated for 48 h in a medium containing EC (5, 10, and 15 μM), Taxol (100 nM), or EC (10 μM) combined with Taxol, followed by continued culture for 10 days. The resulting primary spheroids were digested with trypsin to dissociate them into a single-cell suspension. After counting, the cells underwent secondary plating at same density used the initial spheroid formation. These secondary plates were incubated at 37 °C with 5 % CO_2 for 7–10 days to observe secondary spheroid formation, which was documented with photographs (Chen et al., 2024).

Surface plasmon resonance

The binding kinetics between compound EC and His-tagged PSEN-1 were analyzed by surface plasmon resonance (Biacore T200). PSEN-1 was captured via an anti-His antibody immobilized on a CM5 chip. EC solutions (0.1 nM–10 μM in HBS-EP+ with 1 % DMSO) were injected at 30 μL/min. Data were double-referenced and globally fitted to a 1:1 Langmuir model to obtain ka, kd, and KD. All measurements were performed at 25 °C. The experimental protein is a recombinant soluble truncated domain of human PSEN-1. This construct lacks transmembrane regions and is engineered as a soluble protein to facilitate *in vitro* binding assays.

Lactate dehydrogenase release assay

Cells were incubated for 48 h in a medium containing EC (5, 10, and 15 μM), Taxol (100 nM), or a combination of EC (10 μM) and Taxol. Following the incubation, the supernatant and cell lysates from each well were collected according to the LDH assay kit instruction. The samples were then incubated with the provided detection reagents, including Coenzyme I working solution, substrate buffer, and double-distilled water in the specified ratios. The optical density (OD) was measure at 450 nm. LDH activity (U/l) in the cell culture medium was calculated using formula: (OD value of assay well - OD value of control well) / (OD value of standard well - OD value of blank well) × Standard concentration (0.2 μM) × 1000 (Li et al., 2022).

Annexin V-FITC/PI apoptosis assay

Cells were treated for 48 h with EC (5, 10, and 15 μM), Taxol (100 nM), or a combination of EC (10 μM) and Taxol. After treatment, the cells were washed once with pre-chilled PBS at 4 °C and then detached. The cell suspension was centrifuged at 2000 rpm for 10 min, and the resulting pellets were collected. Each pellet was resuspended in 150 μl of Binding Buffer. Then 2.5 μl Annexin V-FITC stain was added, the sample was mixed thoroughly, and incubated in the dark for 15 min. Prior to analysis, 2.5 μl of PI and 100 μl of Binding Buffer were added sequentially. Apoptotic cells were detected using a flow cytometry (Zhu et al., 2022).

Cell migration assay

A wound healing assay was performed to assess cell migration. A scratch was made in a confluent cell monolayer at time 0 h, and cells were treated with EC (5, 10, and 15 μM), Taxol (100 nM), and a combination of EC (10 μM). Images of the would were captured at 0, 24 and 48 h using an inverted microscope. The acquired images were analyzed with ImageJ software by measuring the scratch area to quantify cell migration (Kaler et al., 2025).

Cell invasion and migration assay

To investigate cell invasion/migration, cells were treated with EC (5, 10, and 15 μM), Taxol (100 nM), or a combination EC (10 μM) combined with Taxol and plated in Transwell inserts. After 48 h treatment, the non-invading/migrating cells on the upper surface of the membrane were removed. The cell had migrated to the lower side of the membrane were fixed with 4 % paraformaldehyde for 10 min, stained with 0.1 % crystal violet solution for 30 min, and washed twice with PBS. The number of migrated cells were imaged and counted under a microscope (Zheng et al., 2024).

Lentiviral transfection

MDA-MB-231 cells were seeded in 6-well plates, and grown to 70 % confluence. Cells were transfected for 24 h using viral supernatant at a multiplicity of infection of 60, supplemented with 8 μg/ml polyvinylpyrrolidone. Following transfection, cells were cultured for an additional 48 h. Stable transfected cells were selected with 2 μg/ml puromycin for 2–3 weeks, and transfection efficiency was verified by RT-qPCR or Western blotting. The following lentiviral vectors were used: For the PSEN-1 OE, pcSLenti-CMV-PSEN1-3 × Flag-PGK-Puro-WPRE3 (Virus ID: H4398); for corresponding OE control, pcSLenti-CMV-MCS-3 × Flag-PGK-Puro-WPRE3 (Virus ID: GL186). For PSEN-1 KD, pCLenti-U6-shRNA (PSEN1)-CMV-Puro-WPRE (Virus ID: Y39882); for KD control, pCLenti-U6-shRNA (NC)-CMV-Puro-WPRE (Virus ID: GL401NC). All viral vectors were provided by OBIO Shanghai (Cowan et al., 2022). All functional assays utilized cell batches whose knockdown efficiency was validated by Western blot.

Establishment of a subcutaneous xenograft tumor model in nude mice

MDA-MB-231 and MDA-MB-231/Taxol cell suspensions (density 1.0 × 10^7/ml) were subcutaneously injected into the axillary region of Balb/C Nude Crlj nude mice (Changsheng Company). Thirty female mice weighing 16–18 g were randomly divided into five groups ($n = 6$). Treatments were administered over 14 days, during which tumor volume and body weight were monitored regularly. EC was delivered by oral gavage at a dose of 20 mg/kg every other day, while Taxol was administered via intraperitoneal injection at a dose of 1mg/Kg twice weekly. After the end of treatment, the mice were anesthetized with isoflurane, and tumor burden were assessed using color Doppler ultrasound. The EC dosage (20mg/Kg) was determined based on the dose-response relationship observed in prior acute toxicity studies. Oral administration was selected due to EC's pharmacokinetic properties as a potential oral drug and its practicality. The dose of Taxol (1mg/Kg) was based on published standard treatment regimens in mouse TNBC models (Jia et al., 2021). Intraperitoneal injection is the commonly used route of administration for paclitaxel in preclinical studies to ensure systemic exposure and reproducible pharmacodynamic effects. The 2-week treatment duration is based on the tumor growth inhibition plateau observed in the pre-experiment and considerations for animal welfare.

Anesthesia Procedure: The anesthetic agent used is isoflurane; the administration route is inhalation general anesthesia; the dosage employed is a 4–5 % concentration of isoflurane, administered via an anesthesia box for induction until the nude mice lose consciousness. Following this, the mice were euthanized, and subcutaneous tumors along with major organs were collected for further analysis. Euthanasia Procedure: The method employed is cervical dislocation. Death is confirmed by observing the cessation of respiration and heartbeat, along with dilated pupils. Tumor growth inhibition rate (TGI) was determined as TGI = (1 - Tumor weight in treatment group / Tumor weight in control group) × 100 %; Tumor volume was calculated using formula: volume= (Tumor length × Tumor width^2) / 2 (Liu et al., 2021). After euthanizing the animals, completely excise the tumor tissue, weigh it, and photograph it. Subsequently, divide each tumor tissue sample into three equal portions: one portion is immediately flash-frozen in liquid nitrogen for protein and RNA extraction (Western blot); one portion is fixed in 4 % paraformaldehyde for paraffin embedding and subsequent histological analysis; the third portion is stored in a specific culture medium for use in other experiments as needed. The experimental protocol was reviewed and approved by the Animal Ethics Committee of Shenyang Medical College (Approval No.: SYYXY2023120801, 8-December-2023). After animals were assigned to groups, a separate researcher not involved in the experimental groupings administered drug injections and measured tumors to ensure experimental blinding.

HE staining

Tissue samples were fixed, and embedded in paraffin. The paraffin blocks were sectioned into approximately 5 μM thick slices. The sections were deparaffinized in xylene rehydrated with a graded ethanol series.

Subsequently they were stained with hematoxylin and differentiated in a differentiation solution for 30 s. After a brief rinse in water, the sections were counterstained with eosin for 30 s. Finally, the section was dehydrated the sections through a graded ethanol series, cleared in xylene, and mounted with a neutral binder. Images were captured using a microscope (De Haan et al., 2021). Histological section evaluation was performed independently by two investigators who were unaware of the experimental groupings. Prepare three consecutive 4-μm-thick paraffin sections from each tumor specimen. From each section, randomly select three non-overlapping fields of view from both the tumor core and peripheral regions for image acquisition and analysis.

Immunohistochemistry staining

Paraffin-embedded sections were deparaffined in xylene and rehydrated with a graded ethanol series. The sections were heated in sodium citrate buffer for 5–10 min for autolysis retrieval using a microwave. Endogenous peroxidase activity was quenched by treating the sections with 3 % H_2O_2 for 10–15 min. Subsequently sections were blocked with 1 % BSA for 20–30 min and them incubated with the primary antibody (PSEN-1) overnight at 4 °C. After washing, an HRP-labeled secondary antibody was applied, and the sections were incubated at 37 °C for 30–45 min. Antigen-antibody complex was visualized using DAB developing solution. Finally, sections were counterstained with hematoxylin and dehydrated through a graded ethanol series, cleared in xylene, and mounted with neutral resin. Images were acquired images using a microscope (Harms et al., 2023). Histological section evaluation was performed independently by two investigators who were unaware of the experimental groupings.

Echocardiography image a micro

Following anesthetized with 1.5 % isoflurane, nude mice were subjected to ultrasound examination using a Color Doppler Ultrasound Diagnostic System (ZS3 SCI/Labus7 Mindray, Shenzhen, China). Body temperature was maintained at a stable level throughout the procedure. The target area was shaved, and a coupling agent was applied to minimize acoustic interference. Multiplanar B-model images of subcutaneous tumors, liver, and kidneys were acquired to document their morphologic characteristics and boundaries (Sultan et al., 2024).

Statistical analysis

Statistical analysis was performed using GraphPad Prism 9.0 software and FlowJo v10.8. The two-tailed Student's *t*-test is used exclusively for comparisons between two groups. One-way ANOVA combined with Tukey's post-hoc test is employed for all comparative experiments involving three or more groups. Data are presented as the mean ± standard deviation from at least three independent experiments. A *p*-value of less than 0.05 was considered statistically significant.

Results

Construction of γ-secretase inhibitor pharmacophores and discovery of EC

The screening process for identifying natural occurring γ-secretase inhibitors, culminating in the discovery of EC is illustrated in Fig. 1. We initially screened 35,143 ligands from eight compound libraries. To prioritize compounds with drug-like properties, we performed an ADME/T (Absorption, Distribution, Metabolism, Excretion, and Toxicity) evaluation based on Lipinski's Rule of Five. This rule state that a compound is likely to have good oral bioavailability if it meets the following criteria: molecular weight (mol_MW) less than 500, Q Plog Po/w less than 5, donor hydrogen bonds (donor HB) less than or equal to 5, and acceptor hydrogen bonds (acceptor HB) less than or equal to 10. This screening identified 19,486 ligands with superior drug-likeness and higher potential for clinical development, which were subsequently subjected to HTVS.

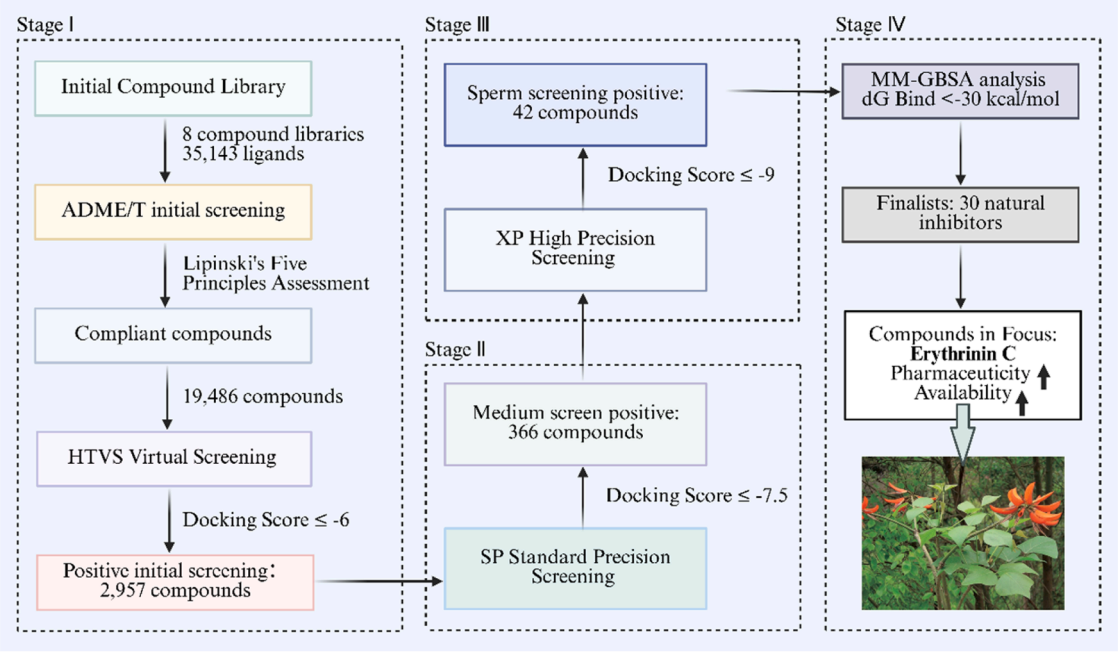

Fig. 1. A flowchart of discovery of natural-source γ-secretase inhibitor Erythrinin C (EC) through virtual screening. A multi-stage virtual screening strategy was employed to identify γ-secretase inhibitors from 35,143 natural compound libraries (n = 35,143). An initial screen based on Lipinski's five rules-based ADME/T selected 19,486 drug-like compounds. These compounds underwent successive rounds of molecular docking with increasing precision: High-Throughput Virtual Screening (HTVS score ≤-6) and Standard Precision (SP score≤-7.5), and Extra Precision (XP score≤-9). The top 42 hits from XP docking were analyzed through MM-GBSA. And 30 compounds with binding free energy analysis (dG<-30 kcal/mol) yielded 30 kcal/mol were selected. From this final group, EC was identified as leading candidate for further investigation.

Based on the HTVS docking results, 17,731 small molecules were found to interact with PSEN-1. Applying a docking score≤-6 kca/moL as the screening criterion, 2957 compounds were identified to meet this standard for future SP docking. From this set, 366 compounds met the more stringent screening criterion of a docking score≤-7.5 kcal/mol and were advanced to extra XP screening, using a threshold of ≤-9 kcal/mol, further narrowed the candidate to 42 compounds. These compounds were subsequently subjected to MM-GBSA analysis to calculate binding free energies, compounds with an MM-GBSA dG Bind<-30 kcal/mol were selected, and after removal of duplicates, 30 unique compounds were retained. The corresponding XP G-Score and MM-GBSA binding free energy results for these 30 compounds are presented in Table 1. Among them, EC was identified as a compound of significant research value due to its favorable drug-like properties and high availability.

Identification of the EC and γ-secretase interaction site and functional consequences

Molecular docking was performed to characterize potential binding patterns of EC within catalytic site of γ-secretase complex (PDB code: 6LR4) (Fig. 2 a-c). The target compound EC exhibited a single peak at a retention time of 8.398 min under both wavelengths, indicating high purity and consistent chromatographic behavior (Fig. 2 d). Results revealed that EC forms four hydrogen bonds with key amino acids LYS380, ALA434, ASP257, and THR147 within the catalytic core of the γ-secretase complex. Hydrogen bonds within the effective distance range from 1.5 Å to 3.5 Å, shorter distances indicate stronger interactions. Notably, the hydrogen bond distances between EC and LYS380, ALA434, and ASP257 ranged from 1.5 Å to 2.5 Å, indicating strong hydrogen bonding interactions. In contrast, the longer hydrogen bond distance with THR147 suggested a comparatively weaker contribution. The surface plasmon resonance kinetic analysis unequivocally confirmed the direct binding of compound EC to PSEN-1. Data indicate moderate-affinity binding (KD = 0.8 ± 0.1 μM), characterized by moderate association kinetics (ka = (2.5 ± 0.3) × 10^4 $M^{-1}s^{-1}$) and fast dissociation kinetics (kd = (2.0 ± 0.2) × 10^{-2} s^{-1}) (Fig. 2 e). The binding response exhibited saturation characteristics with increasing EC concentration, confirming the specificity of the interaction. This result provides direct evidence for EC as a lead compound targeting PSEN-1. Collectively, these interactions demonstrate that the active site of EC exhibits a strong affinity for γ-secretase.

Having established EC as a direct binder of γ-secretase, we next investigated its functional impact on the complex and its downstream signaling molecules, such as PSEN-1, a key subunit of the γ-secretase complex, and Notch pathway. Results showed that in MDA-MB-231 parental cells, medium to high concentrations of EC reduced the protein expression of PSEN-1, Notch-1, Notch-3, and Notch-4 (Fig. 2 f, and supplementary Fig.1 a-d). Next, to explore the potential molecular mechanisms of EC on TNBC cells, the effect of EC on PSEN-1 protein expression was assessed by immunofluorescence staining. PSEN-1 was high expression in control and Taxol cells, and EC effectively downregulated PSEN-1 expression, particularly in the nucleus (Fig. 2 g, and supplementary Fig.1 e). Furthermore, RT-qPCR analysis demonstrated that EC also significantly inhibited the mRNA expression of PSEN-1 (Supplementary Fig.1 f). These results indicate that EC can directly bind g-secretase with high affinity and effectively inhibit Notch pathway activation by downregulating both the expression and activities of its key component proteins.

Table 1
MM-GBSA analysis results.

PubChem ID	Compound Name	XP GScore	MM-GBSA dG Bind (kcal/mol)
11454028	Dibenzazepine	−13.618	−83.15
5497174	Z-VAD(OMe)-FMK	−12.186	−83.52
9843,750	Semagacestat	−11.514	−82.92
5311272	DAPT	−11.47	−84.91
14345578	Torachrysone 8-glucoside	−10.861	−38.94
11582970	Furowanin A	−10.854	−62.89
23675312	Cephapirin sodium	−10.545	−60.61
11662094	Millewanin G	−10.51	−51.89
73364	Calpeptin	−10.495	−63.39
10599228	Kushenol X	−10.486	−48.9
49867930	RO4929097	−10.407	−51.34
14334960	Pyrocatechol monoglucoside	−10.098	−51.99
11154925	Brivanib alaninate	−10.084	−44.91
25050	Ancitabine hydrochloride	−9.791	−40.61
2259	Aurintricarboxylic acid	−9.698	−37.34
10096344	Linagliptin	−9.66	−51.36
71234	Nicaraven	−9.549	−52.03
462382	MG-132	−9.546	−83.51
11199915	Calpain Inhibitor III	−9.431	−66.81
25138012	Lck inhibitor 2	−9.42	−43.33
118647211	Eragidomide	−9.355	−59.45
54698642	MK-2048	−9.344	−48.57
72172	Ubenimex	−9.331	−55.9
44257283	**Erythrinin C**	−9.307	−61.59
443118	Calpain inhibitor I	−9.241	−66.91
138,376,494	Protirelin acetate	−9.177	−52.27
1548994	Silibinin B	−9.123	−53.43
74989	Atovaquone	−9.096	−36.81
16083184	8-Lavandulylkaempferol	−9.091	−53.9
13846690	CID 13846690	−9.055	−57.47

Note: The XP GScore and MM-GBSA free energy for the 30 selected compounds.

EC effectively inhibits the growth of TNBC cells

Using the MTT assay, we determined an IC_{50} value of 8.663 μM for EC in MDA-MB-231 cells (Supplementary Fig.1 p). This anti-proliferative were confirmed by the colony formation assays, which demonstrated that medium to high concentrations of EC significantly inhibited clonogenic growth (Fig. 3 a, and supplementary Fig.1 g). The apoptosis was detected by Annexin V-FITC/PI (Fig. 3 b, and supplementary Fig.1 h), EC induced cell death, as treatment for 48 h increased the proportion of late apoptosis in TNBC cells. Furthermore, tumor spheroid formation was used to assess the stemness. The results revealed that EC treatment resulted in smaller spheroids, suppressed cell stemness, and reduced the self-renewal and clonogenic capacity of TNBC stem cells (Fig. 3 c, and supplementary Fig.1 i). EC also impaired cancer aggressiveness. EC inhibited the migration and invasion of TNBC cells, as demonstrated by transwell assays and validated by a wound healing assay (Fig. 3 d & e, and supplementary Fig.1 j-l). To assess cell damage, LDH release was determined. The increase in LDH release following EC treatment indicated a significant cell membrane damage (Supplementary Fig.1 m). Collectively, these results indicate that EC exerts potent anti-TNBC effects by inhibiting proliferation, inducing apoptosis, disruption the cell cycle, and impairing migration, invasion, and stemness.

EC inhibits γ-secretase activity against TNBC

To elucidate the molecular mechanism by which EC suppresses TNBC progression via γ-secretase inhibition, we established a stably MDA-MB-231 cell line with stable PSEN-1 overexpression or knockout (knockdown state during initial verification). Successful genetic manipulation was confirmed by elevated PSEN-1 expression in the OE group and reduced expression in the KD group at both the protein (Fig. 4 a-c) and mRNA levels (Fig. 4 d & e), validating a successful model. Wound healing assays showed that cells in the OE group exhibited greater migration distances than those in the NC group at 48 h, indicating that PSEN-1 overexpression promotes cell migration (Fig. 4 f & g), whereas KD group exhibited reduced migration distances compared to the NC group after 48 h, indicating that PSEN-1 downregulation effectively inhibits migration in TNBC cells (Fig. 4 h & i). The invasion capacity of cells was assessed using a transwell assay. Compared to the NC group, the OE group showed a significant increase in the number of cells

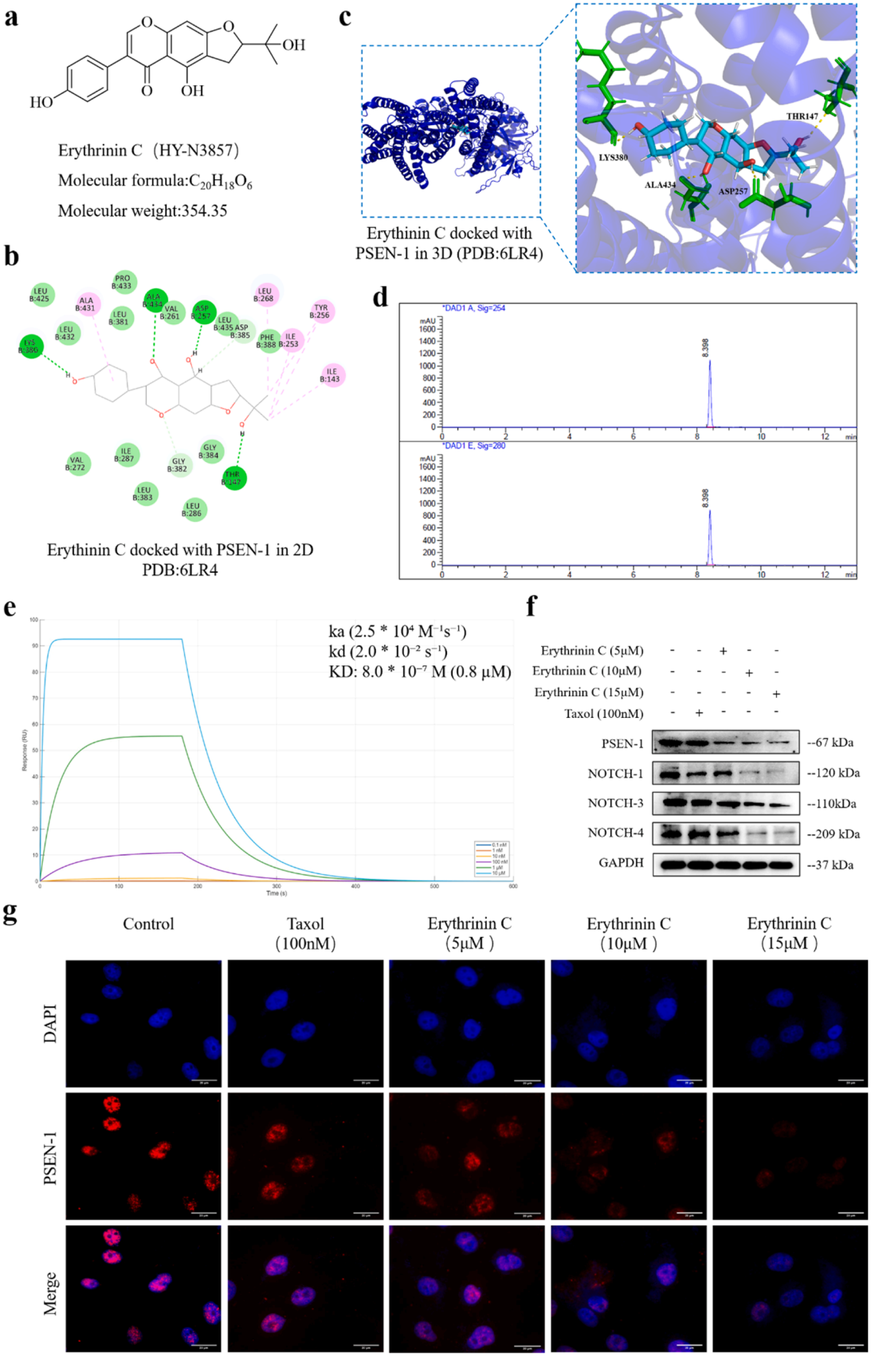

(caption on next page)

Fig. 2. Erythrinin C (EC) directly targets γ-secretase complex and inhibits the Notch signaling pathway. **(a)** Chemical structure of EC. **(b)** 2D docking diagram of predicted binding pose of EC within the PSEN-1. **(c)** 3D molecular docking model of EC bound to the γ-secretase complex; yellow dashed lines indicate hydrogen bonds formed by key amino acids in the EC and γ-secretase complex. **(d)** HPLC chromatogram detected at wavelengths of 254 nm and 280 nm. The chromatograms were acquired on an Agilent 1260 series HPLC system with an Extend-C18 column (5 μm, 4.6 × 150 mm). **(e)** Surface plasmon resonance kinetic analysis unequivocally confirmed the direct binding of compound EC to PSEN-1. **(f)** Representative western blotting showing protein expressions of PSEN-1, Notch-1, Notch-3, and Notch-4 after EC treatment in MDA-MB-231 cells. **(g)** The representative images showing nuclear PSEN-1 expression in MDA-MB-231 cells after 48 h treatment. Data are expressed as mean ± standard deviation. Comparisons among multiple groups were performed using one-way ANOVA followed by Tukey's post hoc test. Data are presented as mean ± SD ($n = 3$ independent experiments). $^{*}p < 0.05$, $^{**}p < 0.01$, $^{***}p < 0.001$, compared with the Control group. $^{\#}p < 0.05$, $^{\#\#}p < 0.01$, $^{\#\#\#}p < 0.001$, compared with the Taxol group.(For interpretation of the references to color in this figure legend, the reader is referred to the web version of this article.).

crossing the matrix membrane, indicating enhanced migration and invasion. In contrast, these capabilities were markedly reduced in the KD group (Fig. 4 j & k, and supplementary Fig.2 a & b). Furthermore, colony formation assay demonstrated that cell proliferation was enhanced in the OE group but impaired in the KD group relative to the NC group, as indicated by a significant increase and decrease in colony number, respectively (Fig. 4 l & m, and supplementary Fig.2 c & d). Immunofluorescence analysis revealed elevated PSEN-1 expression in the nuclei of the OE group compared to the NC group, whereas expression was decreased in the KD group (Fig. 4 n & o, and supplementary Fig.2 e & f). These results confirm the successful establishment of our PSEN-1 genetic modulation model and demonstrate that low expression or gene silencing of PSEN-1 effectively inhibits the proliferation and metastasis of MDA-MB-231 cells.

Using MDA-MB-231 cells with modulation of PSEN-1 expression, we systematically evaluated the effects of combined EC and Taxol treatment on TNBC cell proliferation, migration, and invasion. First, we confirmed high expression of PSEN-1 in the OE group was reduced by EC (10 μM) treatment, while low PSEN-1 expression levels in the KD group (knockdown state during functional experiments) were rescued to near-normal levels by Taxol (100 nM) (Fig. 5 a-c). Western blot validation confirmed that PSEN-1 expression levels in the KD group remained consistently lower than those in the control group (average knockdown efficiency >75 %), demonstrating the validity of functional comparisons in this cellular context (Supplementary Fig. 1 n & o). Functionally, wound healing assay demonstrated that EC treatment inhibited the migration capacity of TNBC cells induced by PSEN-1 OE (Fig. 5 d & f). Conversely, Taxol rescued the migration ability impaired by PSEN-1 KD (Fig. 5 e & g). Transwell assays revealed that EC reduced invasive capacity of OE cells, whereas Taxol increased cell invasion in the KD group (Fig. 5 h & i, and supplementary Fig.2 g & h). Immunofluorescence analysis further corroborated these findings revealing that EC reduced the nuclear expression of PSEN-1 in the OE group, while Taxol restored it in the KD group (Fig. 5 j & k, and supplementary Fig.2 i & j). Finally, tumor spheroid formation assay validated that EC inhibits PSEN-1-mediated migration and proliferation of TNBC cells (Fig. 5 l & m, and supplementary Fig.2 k & l). In summary, these results indicate that Taxol, as an activator of the Notch pathway, promotes the proliferation, migration, and invasion of TNBC cell. Whereas EC counteracts this by exerting anti-TNBC effects through targeting and inhibiting PSEN-1, a key subunit of γ-secretase.

EC reverses the biological characteristics of paclitaxel resistance in TNBC

To determine whether EC counteract Taxol resistance, we first assessed its effect on key Notch pathway-related drug resistance proteins, Western blotting analysis revealed that the combination of EC and Taxol reduced the expression levels of BCRP, CYP3A4, and MDR1, which are associated with resistance in the Notch pathway (Fig. 6 a, and supplementary Fig.3 a-c). We then established a Taxol resistant cell line of MDA-MB-231/Taxol. While these cells showed no morphological from parental cells (Supplementary Fig.3 d). However, after 48 h of Taxol treatment, the viability of parental cells decreased, while that of resistant cells remained robust, yielding a resistance index (RI) of 61.798 (Fig. 6 b), confirming a highly resistant phenotype. To evaluate EC's efficacy, we treated both parental and resistance cells with varying concentrations of EC the MTT assay revealed that EC treatment for 48 h inhibited both cell types, with IC_{50} values of 8.663 μM for parent cells and 9.296 μM for Taxol-resistant cells (Fig. 6 c). This minimal difference in IC_{50} between MDA-MB-231 and MDA-MB-231/Taxol cells indicates that EC retains potent inhibitory activity against Taxol-resistant TNBC cells, suggesting its potent overcome this specific drug resistance.

We further evaluated the combined effect of EC and Taxol on TNBC cell phenotypes. Colony formation assays revealed that compared to the Taxol monotherapy alone, the combination of EC and Taxol had more inhibitory effects on the proliferation of both MDA-MB-231 and MDA-MB-231/Taxol cells (Fig. 6d, and supplementary Fig.3 e). This enhanced anti-proliferative effect was accompanied by a significant increase in late-stage apoptosis of TNBC/Taxol cells, as assessed using Annexin V-FITC/PI staining (Fig. 6 e, and supplementary Fig.3 f). The combination therapy also more potently inhibited metastatic behaviors, as demonstrated by reducing cell migration in wound healing assays (Fig. 6 f, and supplementary Fig.3 g). and impairing both migration and invasion in transwell assays (Fig. 6 g, and supplementary Fig.3 h & i). These results demonstrate that EC synergizes with Taxol to enhance its inhibitory effects on proliferation, migration, and invasion, thereby reducing the resistance of TNBC cells to Taxol. Mechanistic insights revealed that the combination treatment induced significant cellular damage, as indicated by increased LDH release (Supplementary Fig. 3 j). Tumor spheroid formation assays showed that combination therapy suppressed cancer stemness, leading to smaller spheroids and reduced self-renewal and clonogenic capacity of TNBC stem cells (Supplementary Fig.3 k & n).

EC reverses TNBC resistance in vivo

To validate our *in vitro* findings, we investigated the efficacy and safety of EC in reversing TNBC/Taxol resistance using a nude mouse MDA-MB-231/Taxol xenograft model. A schematic diagram of the *in vivo* experiments (Fig. 7 a). Based on an acute toxicity test that established an LD_{50} of 20.24 mg/kg, a maximal dose of 20 mg/kg was selected for the *in vivo* experiments. Compared to Taxol monotherapy, the EC-Taxol combination resulted in a small xenograft tumor volume (Fig. 7 b & c) and yielded superior tumor suppression based on quantitative analysis of tumor volume and weigh inhibition rates (Fig. 7 d, and supplementary Fig.4 g). The tumor growth curve further confirmed that tumor volume gradually decreased in combination group (Fig. 7 e). The treatment also showed a favorable safety profile. Mice in the combination group exhibited an upward trend in body weight compared to the untreated control (Supplementary Fig. 4 a). Single-dose studies cannot fully demonstrate the dose-response relationship of a drug. Building upon this research, we added a high-dose drug treatment group to enhance the scientific rigor of the experiment (Fig. 7 f, Supplementary Fig. 4 b). Color Doppler ultrasound identified a subcutaneous, oval-shaped hypoechoic mass with well-defined borders in nude mice. The subcutaneous tumor volume was significantly smaller in the combination group (Fig. 7 g). Furthermore, the liver and kidneys in all groups exhibited normal morphology with uniform echogenicity, with no abnormal lesions observed (Supplementary Fig.4 c).

HE staining was used to examine the histological structure of

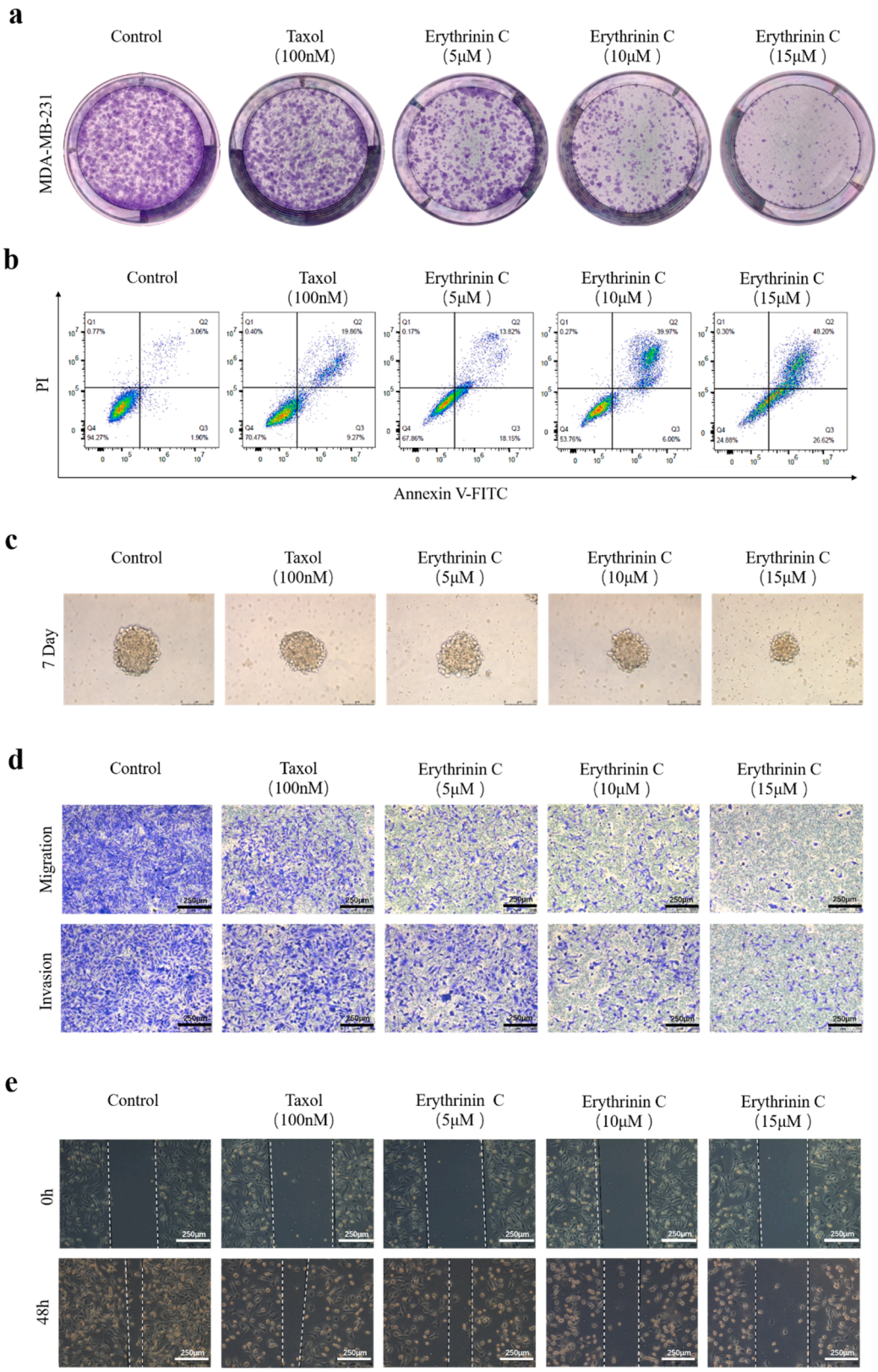

Fig. 3. Anti-tumor effects of Erythrinin C (EC) on MDA-MB-231 cells. **(a)** EC suppresses cell proliferation as shown by the colony formation assay. **(b)** EC-induced late-stage apoptosis, measured by the Annexin V-FITC/PI assay. **(c)** EC, in combination with Taxol, impairs cancer stemness as demonstrated by the tumor spheroid formation assay. **(d)** EC inhibits cell migration capacity in the wound healing assay. **(e)** EC reduces cell migration and invasion in transwell assays. Data are expressed as mean ± standard deviation. Comparisons among multiple groups were performed using one-way ANOVA followed by Tukey's post hoc test. Data are presented as mean ± SD ($n = 3$ independent experiments). $^{*}p < 0.05$, $^{**}p < 0.01$, $^{***}p < 0.001$, compared with the Control group. $^{\#}p < 0.05$, $^{\#\#}p < 0.01$, $^{\#\#\#}p < 0.001$, compared with the Taxol group.

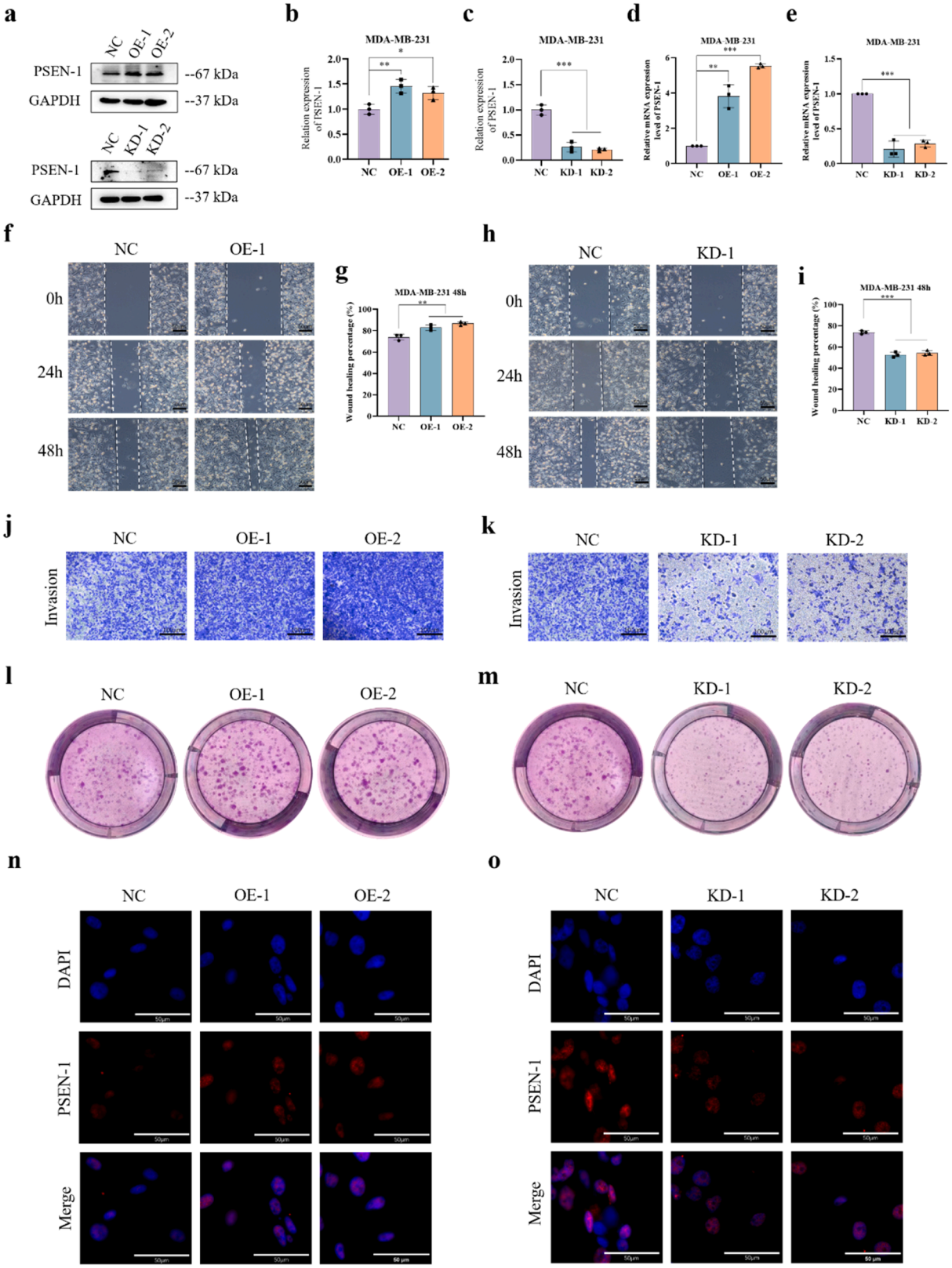

Fig. 4. Silencing the PSEN-1 gene effectively inhibits the proliferation and metastasis in MDA-MB-231 cells. **(a-c)** Validation of PSEN-1 overexpression (OE) and knockout (KD) in MDA-MB-231 cells was confirmed by Western blotting ($n = 3$) and RT-PCR (d&e). Functional consequences were assessed by **(f-i)** wound healing assay for migration **(j & k)** transwell assay for the invasion and **(l & m)** colony formation for proliferation. **(n & o)** Immunofluorescence analysis further verified PSEN-1 protein expression levels in the nuclei of MDA-MB-231 cells. Data are expressed as mean ± standard deviation. Comparisons among multiple groups were performed using one-way ANOVA followed by Tukey's post hoc test. Data are presented as mean ± SD ($n = 3$ independent experiments). *$p < 0.05$, **$p < 0.01$, ***$p < 0.001$, compared to the NC group.

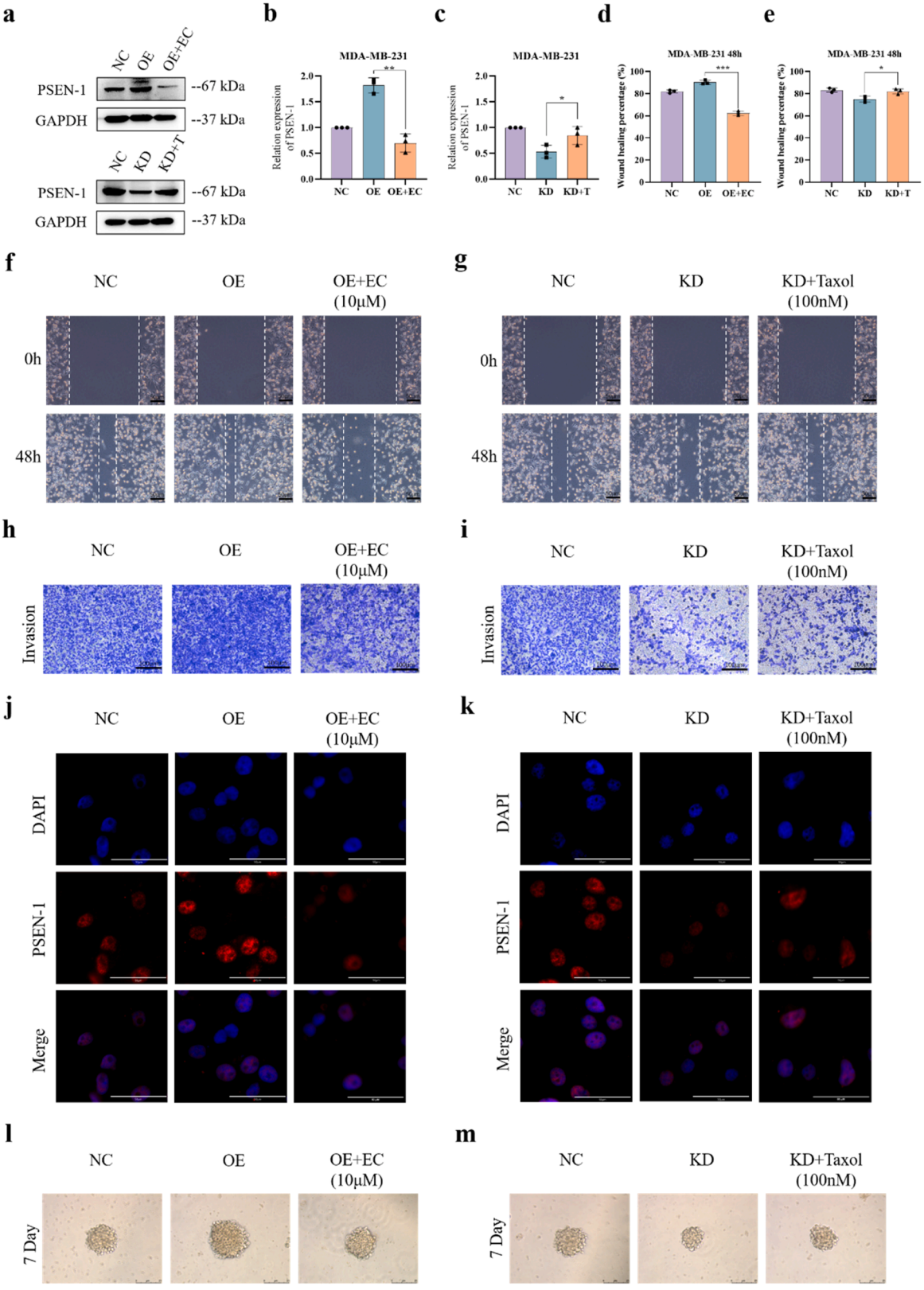

Fig. 5. Erythrinin C (EC) exerts anti- Triple-negative breast cancer (TNBC) effects by inhibiting γ-secretase. (**a-c**) Western blotting analysis of the PSEN-1 protein expression in transfected MDA-MB-231 cells ($n = 3$). **(d-g)** Cell migration capacity assessed by wound healing assay in transfected cells treated with EC or Taxol. **(h & i)** Cell invasion capacity evaluated by transwell assay followed EC and Taxol treatment. **(j & k)** Immunofluorescence analysis of nuclear PSEN-1 protein expression in transfected cells treated with EC or Taxol. **(l & m)** Cancer stemness evaluated by tumor spheroid formation assay in transfected cells treated with EC or Taxol. Data are expressed as mean ± standard deviation. Perform a two-tailed Student's *t*-test. Data are presented as mean ± SD ($n = 3$ independent experiments). $^{*}p < 0.05$, $^{**}p < 0.01$, $^{***}p < 0.001$, compared with the OE or KD groups.

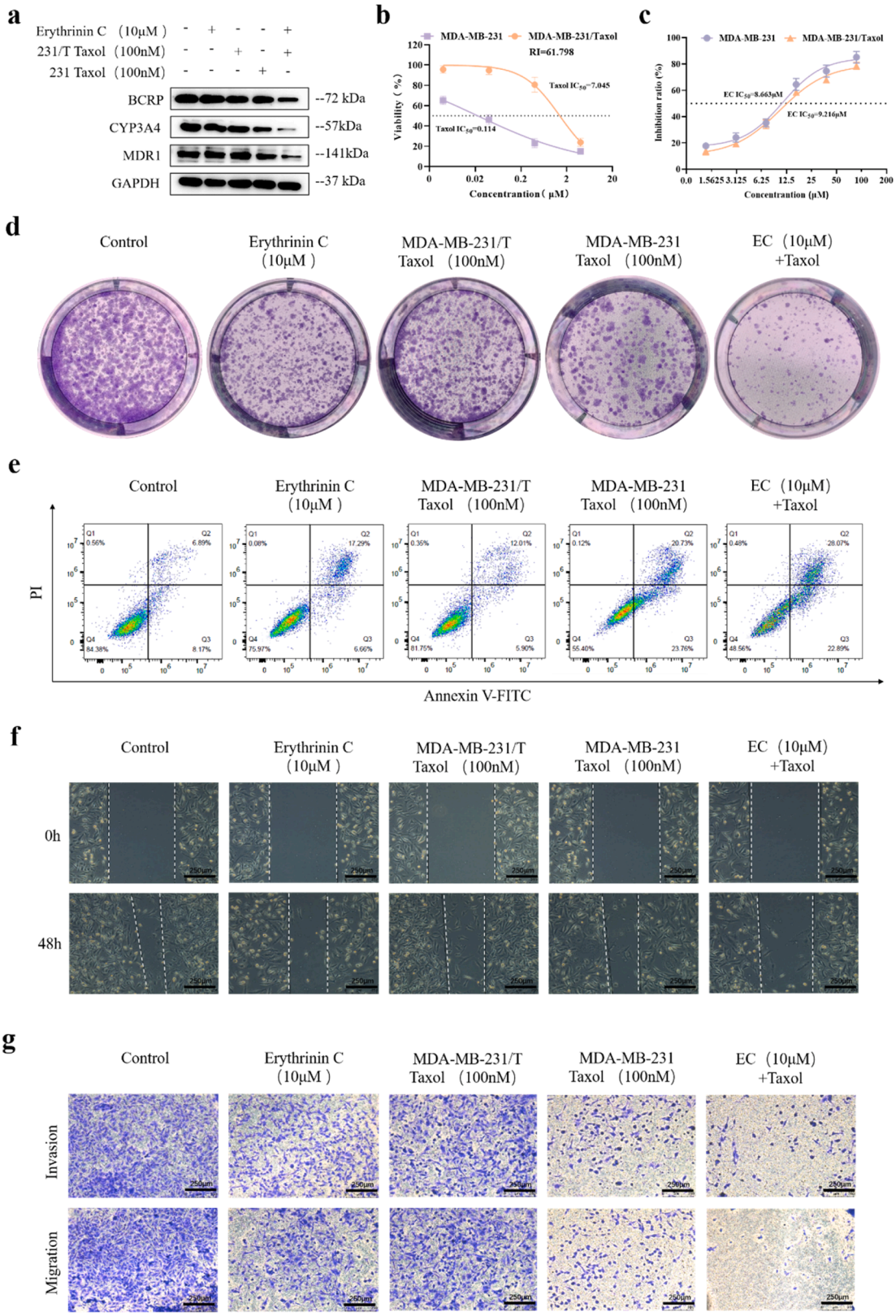

Fig. 6. Erythrinin C (EC) reverses Paclitaxel (Taxol) resistance in Triple-negative breast cancer (TNBC) cells. **(a)** Western blotting analysis of resistance-associated protein expression in TNBC cells after EC combination treatment with Taxol. **(b)** Viability of MDA-MB-231 and MDA-MB-231/Taxol cells treated with Taxol, with calculated IC_{50} values and resistance index. **(c)** Dose-response curves of MDA-MB-231 and MDA-MB-231/Taxol cells treated with EC for 48 h (MTT assay). **(d)** Colony formation assays of MDA-MB-231 and MDA-MB-231/Taxol cells treated with EC, Taxol alone or in combination. **(e)** Analysis of late apoptosis by Annexin V-FITC/PI staining in TNBC cells. **(f)** Cell migration capacity evaluated by wound healing assay after EC and Taxol treatment. **(g)** Cell invasion capacity assessed by transwell assay following combination treatment. Data are expressed as mean ± standard deviation. Data are presented as mean ± SD ($n = 3$ independent experiments). $^{*}p < 0.05$, $^{**}p < 0.01$, $^{***}p < 0.001$, compared with the Control group. $^{\#}p < 0.05$, $^{\#\#}p < 0.01$, $^{\#\#\#}p < 0.001$, compared with the Taxol group.

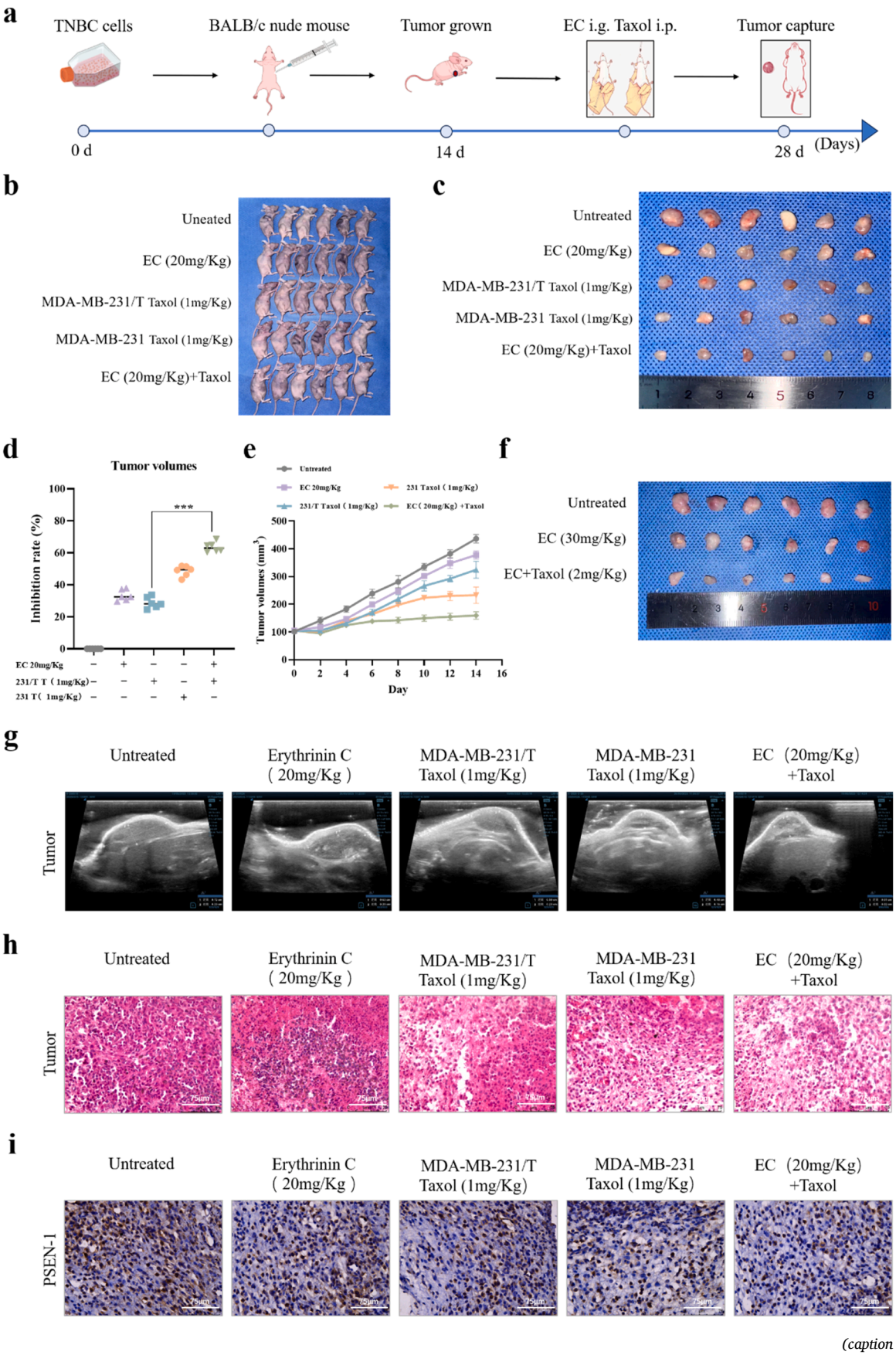

(caption on next page)

Fig. 7. Erythrinin C (EC) enhances the inhibitory effect of Paclitaxel (Taxol) on the growth of Triple-negative breast cancer (TNBC)/Taxol-resistant xenograft tumors. **(a)** Schematic of the subcutaneous breast cancer model establishment and treatment regimen in nude mice: The model was established by injecting MDA-MB-231/Taxol single-cell suspensions into the right axillary region of Balb/c nude mice (i.p. intraperitoneal injection; i.g. oral gavage). **(b & c)** Representative images of excised TNBC cells xenograft tumors from different treatment groups. **(d)** Quantitation of tumor volume suppression rates across the different treatment groups. **(e)** Tumor growth curves throughout drug treatment period. **(f)** Schematic representation of the effect of high-dose therapy on MDA-MB-231/Taxol xenograft tumors. **(g)** Representative Color Doppler ultrasound results images of subcutaneous tumors. **(h)** Representative HE staining images of subcutaneous tumors. **(i)** Representative immunohistochemical staining images of PSEN-1 expression in tumor tissue. Data are expressed as mean ± standard deviation. Perform a two-tailed Student's *t*-test. Data are presented as mean ± SD ($n = 6$ independent experiments). $^{*}p < 0.05$, $^{**}p < 0.01$, $^{***}p < 0.001$, compared with the untreated group. $^{\#}p < 0.05$, $^{\#\#}p < 0.01$, $^{\#\#\#}p < 0.001$, compared with the Taxol group.(For interpretation of the references to color in this figure legend, the reader is referred to the web version of this article.).

subcutaneous tumor tissue and major organs in nude mice. The results showed that untreated tumor tissue exhibited marked nuclear atypia, increased mitotic activity, indicating high malignancy (Fig. 7 h). Compared with the untreated group, no significant histopathological changes were observed in the liver, kidneys, heart, or lungs of nude mice treated with EC-Taxol combination (Supplementary Fig.5 a). Simultaneously, organ indices showed no significant differences in the organ indices of major organs between the combination therapy group and the untreated group, indicating normal organ status (Supplementary Fig.5 b-e).

Ki67 index is a common auxiliary diagnostic indicator for evaluating the benign or malignant nature of breast tumors. Immunohistochemical analysis of Ki67 showed that the EC-Taxol combination mice exhibited a low Ki67 positive rate, characterized by a low staining proportion of stained nuclei (brownish yellow coloration) (Supplementary Fig.4 d & e). Furthermore, the percentage of PSEN-1 positive cells was significantly reduced in the EC-Taxol group compared to the Taxol alone group (Fig. 7 i, and supplementary Fig.4 f). These *in vivo* results indicate that the combination of EC and Taxol significantly inhibits the growth of TNBC/Taxol cell xenografts in nude mice without causing significant toxic reactions. This confirms that EC reverses Taxol resistance in TNBC at the *in vivo* level.

Discussion

Despite advances in the diagnosis and treatment of TNBC, drug resistance remains a significant barrier to therapeutic efficacy (Feng et al., 2024). Naturally derived herbal active ingredients offer a promising avenue for overcoming this challenge. In this study, we constructed the pharmacophore model based on the γ-secretase protein crystal structure and its small-molecule natural ligands. Using this pharmacophore, we screened databases of active components from traditional Chinese medicine and natural products, leading to the first identification of EC as a potential drug candidate. This compound exhibits favorable drug-like properties and high accessibility, underscoring it highly valuable for further investigation.

Preliminary *in vitro* experiments confirmed that EC significantly reduced the survival rate of TNBC cells, demonstrating anti-TNBC activity. To evaluate its potential in reversing Taxol resistance, we investigated the effects of EC on TNBC in both *in vivo* and *in vitro* models. *In vitro* experiments demonstrated that EC inhibits TNBC cell proliferation, invasion and migration, while promoting apoptosis. Based on these findings, EC targets γ-secretase as a therapeutic entry point to further evaluate its ability to reverse TNBC/Taxol resistance. Through *in vivo* pharmacodynamic studies using a nude mouse xenograft subcutaneous tumor model, we validated the inhibitory effect of EC on subcutaneous tumors and demonstrated that EC enhances the inhibitory effect of Taxol on the growth of TNBC/Taxol xenograft subcutaneous tumors. Additionally, we found that the γ-secretase inhibitor EC downregulates the expression of certain tumor resistance genes, including BCRP, CYP3A4, and MDR1, and enhances Taxol's inhibition of TNBC cell proliferation. *In vivo* studies demonstrated that EC potentiates Taxol's inhibitory effect on xenograft tumor growth in nude mice. These results indicate that EC, acting as a γ-secretase inhibitor, enhances Taxol's efficacy in TNBC/Taxol cells and xenograft tumors, providing an effective strategy to overcome TNBC/Taxol resistance.

The activation of the Notch pathway, implicated in TBNC progression, requires three enzymatic cleavages. γ-secretase acts as the final enzyme that cleaves the transmembrane region of the Notch receptor and is essential for Notch signal activation. The C-terminal cleavage product of the transmembrane region of the Notch receptor is cleaved at the S3 site by γ-secretase, releasing NICD into the cytoplasm. NICD translocate to the nucleus, where it binds to the transcription factor CSL and recruits co-activators to initiate transcription of downstream target genes (Jia et al., 2021). PSEN-1 provides the catalytic subunit of γ-secretase and functions as a regulatory component of its cleavage activity (Xu et al., 2025). To genetically validate EC's mechanism, we established MDA-MB-231 cell models with PSEN-1 overexpression and knockout. Our results align with previous studies showing that low PSEN-1 expression effectively inhibits the proliferation and metastasis of TNBC cells. Furthermore, we demonstrate that EC acts as a pharmacological inhibitor of PSEN-1, targeting γ-secretase complex to induce apoptosis in TNBC cells. This study established the first pharmacophore screening model for identifying small-molecule γ-secretase inhibitors and the first to report that EC as a novel, naturally occurring γ-secretase inhibitor. We show that EC targets and inhibits the cleavage activity of γ-secretase, thereby slowing TNBC progression and enhancing TNBC/Taxol chemotherapy sensitivity (Fig. 8).

This study is the first to report EC's anti-TNBC activity and its γ-secretase inhibition mechanism. The vast majority of EC's biological and pharmacological properties remain unknown. Based on its basic isoflavone structure, it is speculated that EC may share pharmacokinetic characteristics common to such natural products, such as moderate oral bioavailability and extensive metabolism via Phase II enzymes (UDP-glucuronosyltransferase enzymes) (Taneja et al., 2016). However, its precise absorption, distribution, metabolism, and excretion profiles require dedicated studies for clarification. Similarly, the safety, adverse reactions, and potential drug interactions of EC when combined with Taxol in human applications warrant further investigation. Future research should systematically evaluate EC's long-term toxicity and organ toxicity effects in preclinical models to explore its potential for clinical translation.

Notably, advancement of high-throughput activity screening technologies has led to the identification of several natural γ-secretase inhibitors. Among these, a few have progressed to clinical trials, this progress provides a foundation for the developing new therapy agents against TNBC drug resistance (Wang et al., 2022). Compared to their chemically synthesized inhibitors, naturally derived γ-secretase inhibitors are predominantly active components found in traditional Chinese medicine or herbal preparations. They offer distinct advantages, including low toxicity, abundant resources, easy accessibility, and enhanced safety. Consequently, these naturally derived γ-secretase inhibitors hold promising potential for combating TNBC and overcoming chemotherapy resistance.

Conclusion

We constructed a γ-secretase pharmacophore model to screen for natural inhibitors and identified that EC as a potent anti-TNBC agent. We demonstrate that EC exerts anti-TNBC effects through targeting and

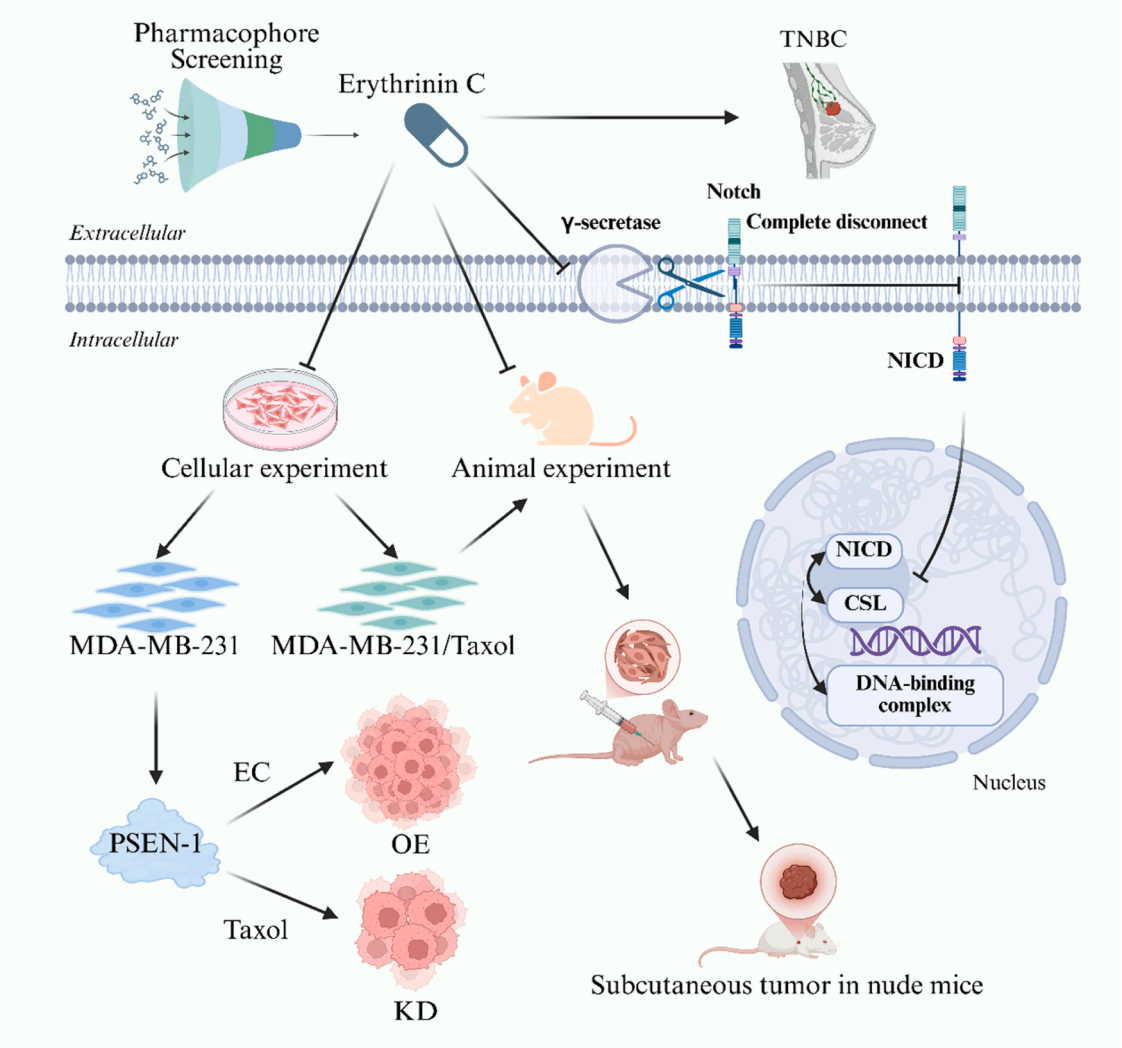

Fig. 8. Schematic diagram of Erythrinin C (EC) targeting γ-secretase to exert anti-Triple-negative breast cancer (TNBC) effects and reverse TNBC/Paclitaxel (Taxol) resistance. Constructing the crystal structure of the γ-secretase protein and the pharmacophore of its small-molecule natural ligands. By screening databases of active components from traditional Chinese medicine and natural products using pharmacophore analysis, potential drug candidates were identified. EC inhibits Notch signaling and NICD activation by suppressing γ-secretase activity, thereby affecting gene expression. The biological characteristics, gene-level effects, and *in vivo* impacts of EC on MDA-MB-231 and MDA-MB-231/Taxol cells were evaluated through both *in vitro* and *in vivo* experiments.

blocking the activity of γ-secretase *in vivo* and *in vitro*. Specifically, blocking γ-secretase activity is achieved by inhibiting PSEN-1 activation. Furthermore, EC effectively reverses TNBC/Taxol resistance, indicating that EC is a promising targeted therapeutic candidate for treating TNBC resistance.

Funding

This work was supported by the grant of National Natural Science Foundation Youth Fund Project (Nos. 82204685); Natural Science Foundation of Liaoning Province, China (Nos. 2023-MHLS-286) to Hui Jia, and by the National Natural Science Foundation of China (Nos. 81970357, 2019; 82270434, 2022) to Ming-Sheng Zhou.

Author statement

Phytomedicine Author Agreement

Dear Editor of Phytomedicine,

We the undersigned declare that this manuscript entitled "Naturally derived Erythrinin C targets γ-secretase signaling to suppress triple-negative breast cancer progression and reverse paclitaxel resistance" is original, has not been published before and is not currently being considered for publication elsewhere.

We confirm that the manuscript has been read and approved by all named authors and that there are not other persons who satisfied the criteria for authorship but are not listed. We further confirm that the order of authors listed in the manuscript has been approved by all of us.

We understand that the corresponding author is the sole contact for the Editorial process. He is responsible for communicating with the other authors about progress, submissions of revisions and final approval of proofs.

Signed by all authors:

CRediT authorship contribution statement

Ke-Fan Yang: Writing – review & editing, Writing – original draft. **Di Wang:** Visualization, Investigation. **Kuo Yao:** Visualization, Investigation. **Ran Xu:** Visualization, Investigation. **Li-Zhi Hu:** Visualization, Investigation. **Yue-Yang Liu:** Visualization, Investigation. **Lu Zhang:** Visualization, Investigation. **Qian Xu:** Visualization, Investigation. **Xin Yang:** Writing – review & editing. **Ming-Sheng Zhou:** Writing – review & editing, Supervision. **Hui Jia:** Writing – review & editing, Supervision,

Funding acquisition, Conceptualization.

Declaration of competing interest

The authors declare that they have no known competing financial interests or personal relationships that could have appeared to influence the work reported in this paper.

Supplementary materials

Supplementary material associated with this article can be found, in the online version, at doi:10.1016/j.phymed.2026.158016.

References

Bianchini, G., De, Angelis, C., Licata, L., Gianni, L., 2022. Treatment landscape of triple-negative breast cancer - expanded options, evolving needs. Nat. Rev. Clin. Oncol. 19 (2), 91–113.

Bisht, A., Tewari, D., Kumar, S., Chandra, S., 2024. Network pharmacology, molecular docking, and molecular dynamics simulation to elucidate the mechanism of anti-aging action of Tinospora cordifolia. Mol. Divers. 28 (3), 1743–1763.

Cowan, MJ., Yu, J., Facchino, J., Fraser-Browne, C., Sanford, U., Kawahara, M., Dara, J., Long-Boyle, J., et al., 2022. Lentiviral gene therapy for Artemis-deficient SCID. N. Engl. J. Med. 387 (25), 2344–2355.

Chen, T., Wen, Y., Song, X., Zhang, Z., Zhu, J., Tian, X., Zeng, S., Li, J., 2024. Rationally designed β-cyclodextrin-crosslinked polyacrylamide hydrogels for cell spheroid formation and 3D tumor model construction. Carbohydr. Polym. 339, 122253.

Feng, M., Santhanam, R.K., Xing, H., Zhou, M., Jia, H., 2024. Inhibition of γ-secretase/notch pathway as a potential therapy for reversing cancer drug resistance. Biochem. Pharmacol. 220, 115991.

Fernandes, RC., Araújo, VA., Giglio, BM., Marini, ACB., Mota, JF., Teixeira, KS., Monteiro, PA., Lira, FS., Pimentel, GD., 2018. Acute epigallocatechin 3 gallate (EGCG) supplementation delays gastric emptying in healthy women: a randomized, double-blind, placebo-controlled crossover study. Nutrients 10 (8), 1122.

Harms, PW., Frankel, TL., Moutafi, M., Rao, A., Rimm, DL., Taube, JM., Thomas, D., Chan, MP., Pantanowitz, L., 2023. Multiplex immunohistochemistry and immunofluorescence: a practical update for pathologists. Mod. Pathol. 36 (7), 100197.

De Haan, K., Zhang, Y., Zuckerman, JE., Liu, T., Sisk, AE., Diaz, MFP., Jen, KY., Nobori, A., Liou, S., Zhang, S., Riahi, R., Rivenson, Y., Wallace, WD., Ozcan, A., 2021. Deep learning-based transformation of H&E stained tissues into special stains. Nat. Commun. 12 (1), 4884.

Jia, H., Liu, M., Wang, X., Jiang, Q., Wang, S., Santhanam, R.K., Lv, C., Zhao, Q., Lu, J., 2021. Cimigenoside functions as a novel γ-secretase inhibitor and inhibits the proliferation or metastasis of human breast cancer cells by γ-secretase/notch axis. Pharmacol. Res. 169, 105686.

Jiang, Z., Ouyang, Q., Sun, T., Zhang, Q., Teng, Y., Cui, J., Wang, H., Yin, Y., Wang, X., Zhou, X., et al., 2024. Toripalimab plus nab-paclitaxel in metastatic or recurrent triple-negative breast cancer: a randomized phase 3 trial. Nat. Med. 30 (1), 249–256.

Kaler, LI., Robitaille, MC., Christodoulides, JA., Calhoun, PJ., Byers, JM., Raphael, MP., 2025. Directing cell phenotype: quantitative single-cell migration assay leveraging tunable extracellular surfaces. Langmuir 41 (22), 13763–13773.

Kwapisz, D., 2021. Pembrolizumab and atezolizumab in triple-negative breast cancer. Cancer Immunol. Immunother. 70 (3), 607–617.

Liu, L., Cui, J., Zhao, Y., Liu, X., Chen, L., Xia, Y., Wang, Y., Chen, S., Sun, S., Shi, B., Zou, Y., 2021. KDM6A-ARHGDIB axis blocks metastasis of bladder cancer by inhibiting Rac1. Mol. Cancer 20 (1), 77.

Li, J., Deng, SH., Li, J., Li, L., Zhang, F., Zou, Y., Wu, DM., Xu, Y., 2022. Obacunone alleviates ferroptosis during lipopolysaccharide-induced acute lung injury by upregulating Nrf2-dependent antioxidant responses. Cell. Mol. Biol. Lett. 27 (1), 29.

Liu, B., Tang, H., Liu, Q., Wang, W., Li, H., Zheng, S., Sun, F., Zhao, X., 2022. Core-shell SERS nanotags-based western blot. Talanta 253, 123888.

Liang, Y., Wang, Y., Zhang, Y., Ye, F., Luo, D., Li, Y., Jin, Y., Han, D., Wang, Z., Chen, B., Zhao, W., Wang, L., Chen, X., Ma, T., Kong, X., Yang, Q., 2023. HSPB1 facilitates chemoresistance through inhibiting ferroptotic cancer cell death and regulating NF-κb signaling pathway in breast cancer. Cell Death Dis. 14 (7), 434.

Roichman, A., Zuo, Q., Hwang, S., Lu, W., Cordova, RA., MacArthur, MR., Boyer, JA., Mitchell, SJ., Powers, J., 2025. Rabinowitz JD. Microbiome metabolism of dietary phytochemicals controls the anticancer activity of PI3K inhibitors. Cell 188 (11), 3065–3080 e21.

Sultan, I., Ramste, M., Peletier, P., Hemanthakumar, KA., Ramanujam, D., Tirronen, A., von Wright, Y., Antila, S., Saharinen, P., Eklund, L., Mervaala, E., Ylä-Herttuala, S., Engelhardt, S., Kivelä, R., Alitalo, K., 2024. Contribution of VEGF-B-induced endocardial endothelial cell lineage in physiological *versus* pathological cardiac hypertrophy. Circ. Res. 134 (11), 1465–1482.

Sharma, P., Stecklein, SR., Yoder, R., Staley, JM., Schwensen, K., O'Dea, A., Nye, L., Satelli, D., Crane, G., Madan, R., O'Neil, MF., Wagner, J., Larson, KE., Balanoff, C., Kilgore, L., Phadnis, MA., Godwin, AK., Salgado, R., Khan, QJ., O'Shaughnessy, J., 2024. Clinical and biomarker findings of Neoadjuvant Pembrolizumab and Carboplatin plus Docetaxel in triple-negative breast cancer: neoPACT phase 2 clinical trial. JAMA Oncol. 10 (2), 227–235.

Tutt, ANJ., Garber, JE., Kaufman, B., Viale, G., Fumagalli, D., Rastogi, P., Gelber, RD., de, A.E., 2021. OlympiA clinical trial steering committee and investigators. Adjuvant Olaparib for patients with BRCA1- or BRCA2-mutated breast cancer. N. Engl. J. Med. 384 (25), 2394–2405.

Tanaka, H., et al., 2018. Two new isoflavones from erythrina suberosa var. Glabrescences. Heterocycles 48 (12), 2661.

Taneja, I., Raju, KS., Wahajuddin, M., 2016. Dietary isoflavones as modulators of drug metabolizing enzymes and transporters: effect on prescription medicines. Crit. Rev. Food Sci. Nutr. 56 (Suppl 1), S95–S109.

Wang, W., Wang, J., Liu, S., Ren, Y., Wang, J., Liu, S., Cui, W., Jia, L., Tang, X., Yang, J., Wu, C., Wang, L., 2022. An EHMT2/NFYA-ALDH2 signaling axis modulates the RAF pathway to regulate paclitaxel resistance in lung cancer. Mol. Cancer 21 (1), 106.

Wang, Z.-J., Zhan, X.-Y., Ma, L.-Y., Yao, K., Dai, H.-Y., Kumar Santhanam, R., Zhou, M.-S., Jia, H., 2024a. Activation of the γ-secretase/NICD-PXR/notch pathway induces taxol resistance in triple-negative breast cancer. Biochem. Pharmacol. 230 (Pt 2), 116577.

Wang, D., de Los Reyes 3rd., F.L., Ducoste, JJ., 2023. Microplate-based cell viability assay as a cost-effective alternative to flow cytometry for microalgae analysis. Environ. Sci. Technol. 57 (50), 21200–21211.

Wang, K., Zhang, P., Sun, H., Cui, S., Ao, L., Cui, M., Xu, X., Wang, L., Xu, Y., Wang, G., Wang, H., Hao, H., 2024b. Dual-function natural products: farnesoid X receptor agonist/inflammation inhibitor for metabolic dysfunction-associated steatotic liver disease therapy. Chin. J. Nat. Med. 22 (11), 965–976.

Xu, R., Yang, X., Yao, K., Yang, K.-F., Hu, L.-Z., Zhan, X.-Y., Zhou, M.-S., Jia, H., 2025. Key subunits of γ-secretase complex and breast cancer progression: biological function, regulation mode and therapeutic potential. Biochim. Biophys. Acta Rev. Cancer 1880 (4), 189386.

Yang, W., Wang, Y., Huang, Y., Yu, J., Wang, T., Li, C., Yang, L., Zhang, P., Shi, L., Yin, Y., Tao, K., Li, R., 2023. 4-Octyl itaconate inhibits aerobic glycolysis by targeting GAPDH to promote cuproptosis in colorectal cancer. Biomed. Pharmacother. 159, 114301.

Yang, K.-F., Zhang, J.-Y., Feng, M., Yao, K., Liu, Y.-Y., Zhou, M.-S., Jia, H., 2024. Secretase promotes AD progression: simultaneously cleave notch and APP. Front. Aging Neurosci. 16, 1663–4365.

Yao, K., Zhan, X.-Y., Feng, M., Yang, K.-F., Zhou, M.-S., Jia, H., 2024. Furin, ADAM, and γ-secretase: core regulatory targets in the Notch pathway and the therapeutic potential for breast cancer. Neoplasia 57, 101041.

Zheng, D., Wei, Z., Zhang, C., Liu, W., Gong, C., Wu, F., Guo, W., 2024. ZNF692 promotes osteosarcoma cell proliferation, migration, and invasion through TNK2-mediated activation of the MEK/ERK pathway. Biol. Direct 19 (1), 28.

Zhu, S., Li, X., Dang, B., Wu, F., Wang, C., Lin, C., 2022. Lycium Barbarum polysaccharide protects HaCaT cells from PM2.5-induced apoptosis via inhibiting oxidative stress, ER stress and autophagy. Redox Rep. 27 (1), 32–44.

Zheng, X., Peng, P., Wang, Y., Bian, L., Zhao, K., Shi, A., Jiang, Z., Zhao, L., Jiang, J., Zhang, S., 2025. The impact of exercise during radiotherapy on treatment-related side effects in breast cancer patients: a systematic review and meta-analysis. Int. J. Nurs. Stud. 163, 104990.

Zucha, D., Kubista, M., Valihrach, L., 2021. Tutorial: guidelines for single-cell RT-qPCR. Cells 10 (10), 2607.

Zhang, Y., Chen, H., Mo, H., Zhao, N., Sun, X., Liu, B., Gao, R., Xu, B., Zhang, Z., Liu, Z., Ma, F., 2025. Distinct cellular mechanisms underlie chemotherapies and PD-L1 blockade combinations in triple-negative breast cancer. Cancer Cell 43 (3), 446–463 e7.

Zhu, S., Wu, Y., Song, B., Yi, M., Yan, Y., Mei, Q., Wu, K., 2023. Recent advances in targeted strategies for triple-negative breast cancer. J. Hematol. Oncol. 16 (1), 100.